International Research Journal of Engineering and Technology (IRJET) e-ISSN: 2395-0056
Volume: 07 Issue: 12 | Dec 2020 www.irjet.net p-ISSN: 2395-0072

DESIGN AND IMPLEMENTATION OF BATTERY MANAGEMENT SYSTEM IN ELECTRIC VEHICLE

Vinay Kumar[1], Dr. M N Dinesh[2]

[1]PG student, EEE Dept., RV College of Engineering, Bengaluru, Karnataka, India
[2]Associate Professor, EEE Dept., RV College of Engineering, Bengaluru, Karnataka, India

---

Abstract - *The main objective of the work is to protect the battery cells from abuse and damage. It extends the battery life as long as possible and it makes sure the battery is always ready to be used. Implementation of active clamp forward converter for active cell balancing, Design a new BMS platform based on available dedicated integrated circuits and microcontrollers targeting fast sampling, high accuracy, low consumption and low cost. The BMS topology and active forward converter was simulated in Or CAD, TINA software and MATLAB Simulink software. The simulation of the active forward converter showed that for an input voltage of 40V the output voltage was 3.3V, with an efficiency of 90%. The ripple in the converter is limited to less than 5%. The BMS topology is reviewed and the PCB was printed, then the PCB is tested with connecting battery stack for both charging and discharging process of active cell balancing.*

Key Words: Active clamp forward converter, Li-ion batteries, active cell balancing, etc.

1. INTRODUCTION

The increasing use of lithium-based battery cells in electric and hybrid vehicles has presented many challenges in terms of system design and safe use of the cells [7]. These challenges include the unique characteristics of the battery chemistry that requires new technologies for monitoring and maintaining the battery cells during use, real time decision making based on measured parameters, and optimizing the overall system to obtain the maximum performance [8].

The balancing of a lithium-based battery system [9-11] has one very large benefit. As the batteries are charged and discharged their capacity is reduced. The unbalanced discharging and charging of cells accelerates the time before the cell capacity is diminished to the point of the system being no longer useful or decreases the time before failure. The equal charging and discharging of the individual cells allows the end user to obtain the maximum energy and life out of the battery system as a whole, eventually saving cost and environmental resources [12-13]. While battery energy capacity, weight, and reduced harm to the environment are continually being improved, the technology is still slower progressing than the technology using the batteries as an energy source. Therefore, the utilization of the present battery technology is of great importance.

The output power requirement of the proposed converter is 100W. 3.13V to 3.46V and 30A are the full load converter output voltage and current specifications. An input voltage range is specified for the stable operation of the proposed topology. The minimum input voltage supplied to the converter is 39.6V. The maximum input voltage allowed for the stable operation is 52.8V. The maximum duty ratio for the converter operation is 0.6. UCC2897A PWM controller is used. In the BMS system the PWM signals were given to the both primary and secondary side switches from the EMB1499Q IC. The signals to the dc-dc converter IC were from EMB1428 which is controlled by the microcontroller.

1.1 Li-ion battery

An electric battery is a device consisting of one or more electrochemical cells with external connections provided to power electrical devices such as flashlights, smartphones, and electric cars. When a battery is supplying electric power, its positive terminal is the cathode and its negative terminal is the anode. The terminal marked negative is the source of electrons that will flow through an external electric circuit to the positive terminal. Battery cells are connected in series and parallel configuration to obtain required output voltage and current from battery pack. The parameters that are to be considered while choosing batteries are battery capacity (Ah), battery voltage, battery charging and discharging rate, efficiency, power density, cost and lifecycle. This provides the comparison of various parameters of different batteries for electric vehicle.

Lithium is the lightest metal with the greatest electrochemical potential and the largest energy density per weight of all metals found in nature. Using lithium as the anode, rechargeable batteries could provide high voltage, excellent capacity and a remarkably high-energy density. However, lithium is inherently unstable, especially during charging. Therefore, lithium ions have replaced lithium metals in many applications because they are safer than lithium metals with only slightly lower energy density. Nevertheless, certain precautions should be made during charging and discharging.

1.2 Active Cell Balancing

In Passive cell balancing the excess charge was not made used of, hence it is deemed to be inefficient. Whereas in active balancing the excess charge form one cell is transferred to another cell of low charge to equalize them.

This is achieved by utilizing charge storing elements like Capacitors and Inductors. There are many methods to perform Active cell balancing lets discuss the commonly used ones.

Charge Shuttles (Flying Capacitors)

This method utilizes capacitors to transfer charge from high voltage cell to low voltage cell. The capacitor is connected through SPDT switches initially the switch connects the capacitor to the high voltage cell and once the capacitor is charged the switch connects it to the low voltage cell so that the charge from the capacitor flows into the cell. Since the charge is shuttling between the cells this method is called as charge shuttles. The below Figure 1 shows the charge shuttles.

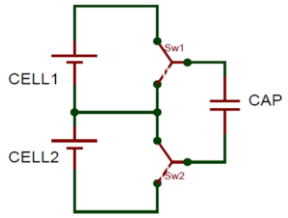

Figure 1 Active cell balancing

2. Battery Management Systems (BMS)

There are different types of BMSs that are used to avoid battery failures. The most common type is a battery monitoring system that records the key operational parameters such as voltage, current and the internal temperature of the battery along with the ambient temperature during charging and discharging. The system provides inputs to the protection devices so that the monitoring circuits could generate alarms and even disconnect the battery from the load or charger if any of the parameters exceed the values set by the safety zone.

The battery is the only power source in pure electric vehicles. Therefore, the BMS in this type of application should include battery monitoring and protection systems, a system that keeps the battery ready to deliver full power as it is necessary and a system that can extend the life of the battery. The BMS should include systems that control the charging regime and those that manage thermal issues.

In a vehicle, the BMS is part of a complex and fast-acting power management system. In addition, it must interface with other on-board systems such as the motor controller, the climate controller, the communications bus, the safety system and the vehicle controller.

External charger is connected to the battery by contactor and it is control by battery control unit. Loads like ECU engine and controller are connected to the battery by DC/DC converter to give sufficient supply required to that by using contactor. BMS control the current, temperature and voltage in each cell in the battery. Cell: The basic electrochemical unit used to generate electrical energy from stored chemical energy or to store electrical energy in the form of chemical energy. A cell consists of two electrodes in a container filled with an electrolyte. Two or more cells connected in an appropriate series/parallel arrangement to obtain the required operating voltage and capacity for a certain load. The term battery is also frequently used for single cells. This terminology will also be adopted in this thesis, except at that time of distinction between cells and batteries is needed. A good example is a battery pack, which consists of several cells connected in series and/or parallel. BMS Block Diagram is shown in Figure 2.

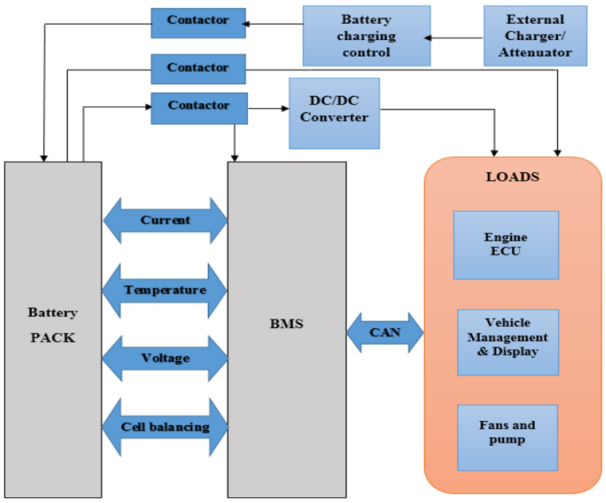

Figure 2 BMS Block Diagram

3. Active clamp forward converter operation

The low side active clamp circuit employed forward converter is as shown in Figure 3 The switch M2 and capacitor C1 form the low side clamp circuit [21]. This circuit absorbs the surge energy and performs core reset completely with reduced voltage stress across the primary switch M1. The energy transfer to the secondary winding occurs throughout the power transfer mode. The stored energy in the primary winding is transferred to the capacitor C1 during the reset time. The clamp switch in high side configuration is the N channel device. High side clamp circuit is preferred for the converter applications requiring the lowest voltage stress. More component choices are available for high side clamp since the N channel device is used. The clamp switch in low side configuration is a P channel device [24].

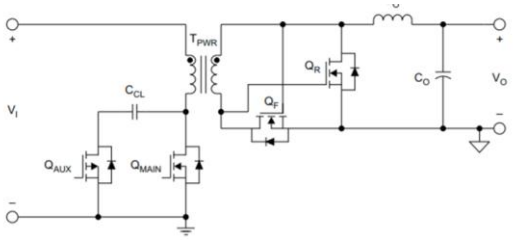

Figure 3 Active clamp forward converter

Mode 1: t0-t1

During this state shown in Figure 4 power is transferred to the secondary as the main switch, QMAIN, is conducting and, under the right conditions, has just turned on. The primary current is flowing through the channel resistance of QMAIN and is made up of the transformer magnetizing current plus the reflected secondary current. On the secondary side, the forward synchronous rectifier, QF, is on and carrying the full load current. In the previous state, the load current was in the synchronous rectifier, QR, which is turning off as QF is being turned on so they are both subjected to some turn-on loss.

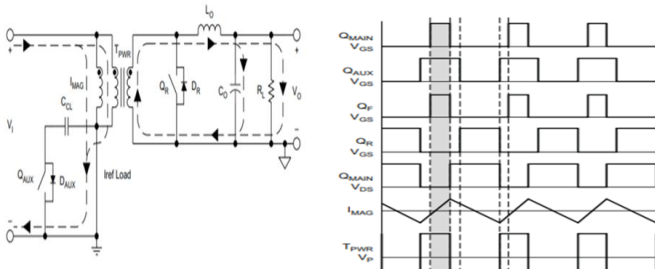

Figure 4 t0 to t1 Power Transfer Interval

Mode 2: t1-t2

This is the resonant state shown in Figure 5 that occurs within each switching cycle. During this state QMAIN has turned off under ZVS and the primary current remains continuous as it first charges up the drain to source capacitors of QMAIN and discharges the drain to source capacitor of QAUX. Then it is diverted through the body diode, DAUX, of the clamp switch, QAUX. Because of the direction of the primary current flowing through DAUX, QAUX must be a P-channel MOSFET (body-diode pointing down) for low-side active clamp applications. Since the secondary load current is freewheeling, there is no reflected primary current, so the only current flowing through DAUX is the transformer magnetizing current. Therefore the body-diode conduction loss of QAUX is minimal and the conditions are set for QAUX to turn on under ZVS. The delay time between QMAIN turn-off and QAUX turn-on, also known as the resonant period, distinguishes the active clamp from other single ended transformer reset methodologies. On the secondary side, the voltage across the secondary winding has collapsed as it reflects the primary side voltage. This should result in a near zero voltage transition of the current into the body diode of QR as the winding reverses voltage polarity.

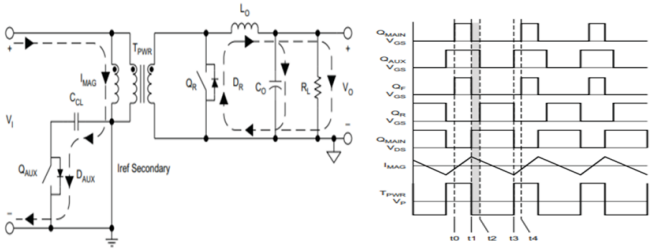

Figure 5 t1 to t2: Resonant Interval

Mode 3: t2-t3

This is the active clamp state shown in Figure 6, the transformer primary is reset. Although the schematic of Figure 3.5 shows an immediate reversal of the primary current, the transition from positive to negative current flow is actually smooth and had really begun during the previous state as the magnetizing current had reached its maximum positive peak value. On the primary side, QAUX is now fully turned-on as the difference between the input voltage, VIN, and the clamp capacitor voltage is now applied across the transformer primary. QAUX is subject to minimal conduction loss as only the magnetizing current is flowing through the channel resistance. Conversely, on the secondary side, QR is carrying the full load current through its channel resistance and is experiencing high conduction loss.

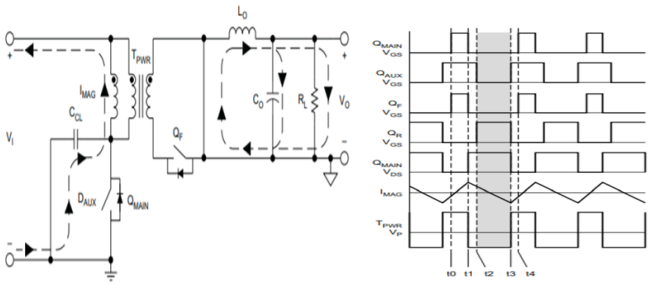

Figure 6 t2 to t3: Active Clamp Reset Interval

Mode 4: t3-t4

During this state QAUX has turned off under ZVS and the magnetizing current starts to decrease the voltage on the drain to source parasitic capacitor of the QAUX and QMAIN FETs resulting in a voltage decrease on the QMAIN drain to source capacitance and a negative voltage increase on the drain to source capacitance of QAUX. This change in voltage results in a decrease in voltage across the primary winding and the change in voltage is reflected to the secondary. Changing the secondary voltage requires current to change the drain to source capacitance of QF and the gate capacitances of both QF and QR. This results in the primary side magnetizing current being diverted to the secondary to alter the voltage on the gate to source capacitances of the secondary switches and slows the rate of change of voltage on QMAIN. In this mode, primary voltage Vp remains zero. At the secondary side, the intrinsic diodes of the forward and freewheeling switches S3 and S4 are forward biased as shown in Figure 7.

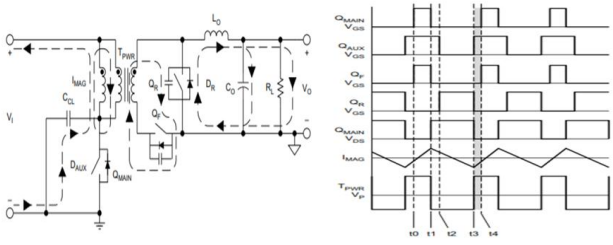

Figure 7 t3 to t4: Qaux "OFF" to Qmain "ON"

4. Design of active clamp forward converter

The design of the main transformer is as follows: -
Calculation of the total output power of the converter
$P_{out}=P_{out1}+P_{bias}+P_{bias1}$
Where, Pout1 is the required output power
Pbias is required power for PWM-ICs and OPAMP circuits
Pout is the total output power the transformer is designed for
$P_{out}=V_{out}\times I_{out}$
$= 3.3\times30 = 100$ W
$P_{bias}=V_{bias}\times I_{bias}$
$= 12\times0.1 = 1.2$ W
Calculation of input pulsating current and primary current
Input pulsating current

$$I_p=\frac{P_{out}}{Efficiency\times Vin_{min}\times D_{max}}$$
$= 104.2 \div (0.9\times36\times0.6) = 5.36$A

$$\text{Average primary current} = \frac{P_{out}}{Efficiency\times Vin_{min}}$$
$= 104.2 \div (0.9\times36)$
$= 3.216$

Calculation of area product:-The power transformer's size is calculated by the Area product method [3]. The area product is calculated before the transformer core selection.
$A_p = A_c.A_w$
Where, A_c: Core cross section area, A_w: Window area
A_p: Area product $A_p=\frac{\sqrt{D_{max}}\times P_{out}\left(1+\frac{1}{Efficiency}\right)}{B_m F_{sw} K_w J 10^{-6}}$
Where,
Pout: Output Power
Kw: Window Factor.
Fsw : Switching Frequency
Bm: Flux Density (Tesla)
J: Current Density (Amp/mm^2)
Dmax: Maximum Duty Cycle
Kw, Bm & J are used for the optimum design of the transformer. The optimum design is finally decided by the small size & lower power dissipation of the transformer. Optimized values of Kw, Bm & J are used in the design. Normally, Window Factor (Kw) varies from 0.3 to 0.5. Flux Density (Bm) depends on the core material. It varies from 0.12 to 0.2. Current Density varies from 3Amp/mm^2 to 6Amp/mm^2 [3]. The chosen values for the design are as follows: Flux density, Bm=0.12T; Current density, J= 6 A/mm^2; Window factor, Kw = 0.4.
Substituting the values into equation (4.8), calculated area product is,

$$A_p = \frac{\sqrt{0.6}\times104.2\times\left(1+\frac{1}{0.9}\right)}{0.4\times6\times10^{-6}\times0.12\times250\times10^3}$$
$=2.366\times10^3\ mm^4$.

Requirement of core selection Appropriate core is selected having area product value larger than the calculated value of the Ap [19]. The specifications of the core selected are as follows:

Core selected: PA0810NL.The selected core has the cross-sectional area Ac = 136 mm^2 and window area Aw = 54.139 mm^2.
Ap = Ac. Aw
$= 7.37\times10^3\ mm^4$
Calculation of primary winding turns

$$N_p=\frac{Vin_{min}\times D_{max}}{B_m A_c\times10^{-6} F_{sw}}$$

$$N_p=\frac{36\times0.6}{0.12\times136\times10^{-6}\times250\times10^3}=6$$

Calculation of secondary winding turns

$$\frac{N_s}{N_p}=\frac{Vout}{Vin_{min}\times D_{max}} \quad ; \quad \frac{N_s}{N_p}=\frac{3.3}{36\times0.6}=0.153$$

Ns = 0.153× 6 = 1
Transformer primary winding is wound for 6 turns and the secondary winding is wound for 1 turn
Diameter of wire

$$dn = 0.127 * 92^{\frac{36-n}{39}}$$
$= 0.3211$

Cross-sectional area of AWG

$$Aw\_28\ AWG = \frac{\pi}{4} d\,n^2 = 0.081$$

$$\text{Primary no of strands} = \frac{Aw\_Np}{Aw\_28\ AWG}$$
$= \frac{2.44667}{0.081}$
$= 26$ strands

$$\text{Secondary no of strands} = \frac{Aw\_Ns}{Aw\_28\ AWG}$$
$= \frac{5.634}{0.081}$
$= 70$ strands

Calculation of winding inductance for nominal AL value
Primary inductance $Lp = AL * Np^2$
$= 6680 * 52$
$= 167$ uH
Secondary inductance $Ls = AL * Ns^2$
$= 6680 * 12$
$= 60$ uH
Primary winding is wound for 4 turns each turn has 26 strands. Secondary winding is wound for 1 turns, each turn has 70 strands. The primary inductance is equal to 167uH and secondary inductance is equal to 60 uH.

Output filter design
The output filter section consists of an inductor in series for current smoothening and capacitor in parallel for a reduction in the output ripple voltage.
Calculation of output inductance
The maximum ripple content in output current is assumed to be 15%. The minimum duty cycle Dmin allowed for the converter operation is calculated.

$$L_O=\left(\frac{V_O}{\Delta I_{LO}\times I_O\times f_{OSC\_MIN}}\right)\times(1-D_{MIN})$$
$= 2.281$uH

Calculation of Output Capacitance

$$C_O = \frac{L_O \times \left(I_{STEP\_MAX}^2 - I_{STEP\_MIN}^2\right)}{\left(V_{OS\_MAX}^2 - V_{OS\_MIN}^2\right)}$$

= 671.642uH

Calculation of active clamp capacitance, Clamp capacitance is calculated for a 20% voltage ripple.

$$C_{CL} > 10 \times \left(\frac{(1-D_{MIN})^2}{L_{MAG} \times (2 \times \pi \times f_{SW})^2}\right)$$

= 24.699nF

5. SIMULATION RESULTS

The Ziegler-Nichols' method PI controller is included in the feedback path of the converter for the closed-loop operation. This voltage is compared with the constant voltage of 3.25V in the error amplifier. The compensated value from the error amplifier fed to the PI block. The PWM pulses are generated and are fed as gating signals to active clamp and main MOSFET as shown in Figure 8.

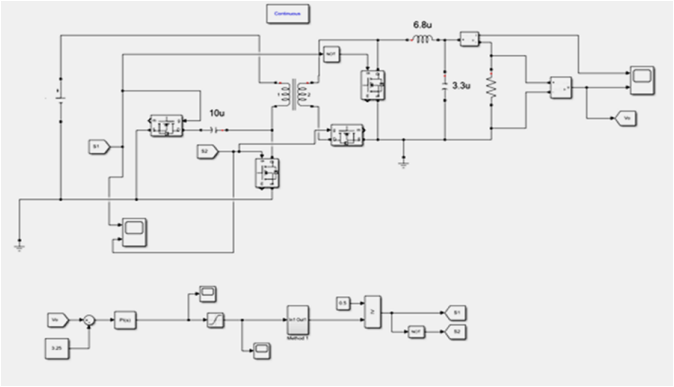

Figure 8 Closed-Loop Active Clamp Forward Converter

The conventional forward converter is simulated using MATLAB. The output voltage waveform of the conventional forward converter is as shown in Figure 9.

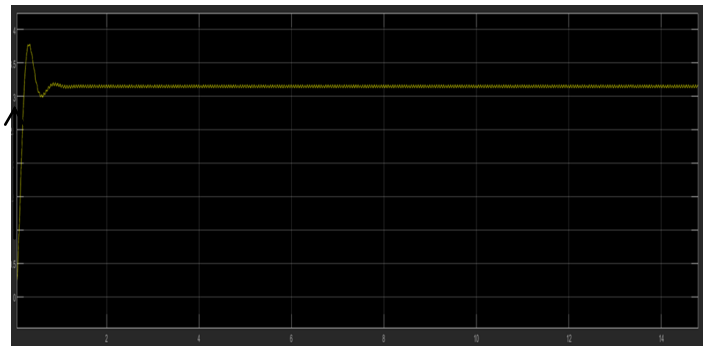

Figure 9: Output voltage of conventional converter without active clamp.

An output voltage of 3.3V with a ripple of 0.15 is obtained for an input of 40V and 0.6 duty ratio.

The proposed battery management system (BMS) topology is tested and hardware waveforms are obtained using DSO. Figure 10 shows the primary side main MOSFET and, secondary side forward MOSFET Qf and freewheeling MOSFETS Qr gate waveforms for nominal input voltage and full load conditions of 40V. The complementary gate signals are generated for forward and freewheeling MOSFET. Figure 11 shows the Vgs of aux/clamp MOSFET.

Figure 10 Vgs of Primary Main MOSFET (pink), Secondary Forward MOSFET (blue), Freewheeling MOSFET (yellow).

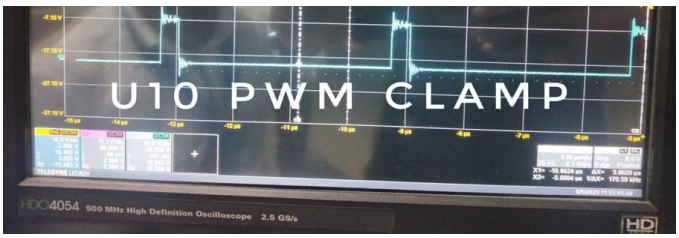

Figure 11 Vgs of aux/clamp MOSFET.

6. CONCLUSIONS

The purpose of this project was to examine an active method of battery cell balancing for lithium based battery systems. Topologies were reviewed to determine the design for the hardware that was ultimately constructed and tested. Simulations were also performed as a metric to validate the hardware operation. Overall, the active balancing system met the goal of being more effective at maintaining the system voltage and reducing the time taken to balance the cells. The battery cell voltages were sensed and the temperatures of the battery cell were sensed. In this work, active clamp forward converter was adopted. A high-speed PWM controller provides PWM pulses for the switches of the converter. Complementary gating signals were provided through the EMB1499Q IC. The hardware implementation includes converter along with startup, overvoltage and under voltage protection circuits

REFERENCES

[1] Thiruvonasundari Duraisamy, Deepa kaliyaperumal, "Active cell balancing for electric vehicle battery management system", International Journal of Power Electronics and Drive System (IJPEDS) Vol. 11, No. 2, June 2020, pp. 571~579

[2] Kailong LIU, Kang LI, Qiao PENG, Cheng ZHANG "A brief review on key technologies in the battery management system of electric vehicles." Frontiers of Mechanical Engineerin. 14, 47–64 (2019).

[3] Ali Farzan Moghaddam, Alex Van den Bossche "An Active Cell Equalization Technique for Lithium Ion Batteries Based on Inductor Balancing", 9th International Conference on Mechanical and Aerospace Engineering (ICMAE),2018.

[4] Texas instruments "Active Chipset Reference Design Guide" Literature Number: SLUUAS6A December 2013–Revised September 2017

[5] Meng Di Yin, Jiae Youn, Jeonghun Cho, and Daejin Park* "MCU-based Battery Management System for Fast Charging of IoT-based Large-Scale Battery-Cells", International Journal of Applied Engineering Research ISSN 0973-4562 Volume 12, Number 7 (2017) pp. 1329-1333 © Research India Publications.

[6] Mr. Rohit S. Dhaigude1 , Mr. Javed H. Shaikh2 "BATTERY MANAGEMENT SYSTEM IN ELECTRIC VEHICLE", 7th international conference on recent trends in engineering, science & management 2017.

[7] M.S. Yusof1, S.F. Toha2, a, N.A Kamisan3, N.N.W.N. Hashim4, M. A. Abdullah5, "Battery Cell Balancing Optimization for Battery Management System", International Conference on Mechanical, Automotive and Aerospace Engineering 2016.

[8] Changhao Piao, Zhaoguang Wang, Ju Cao, Wei Zhang, and Sheng Lu, "Lithium-Ion Battery Cell-Balancing Algorithm for Battery Management System Based on Real-Time Outlier Detection" Hindawi Publishing Corporation Mathematical Problems in Engineering Volume 2015, Article ID 168529.

[9] Costinett, D., Hathaway, K., Rehman, M. U., Evzelman, M., Zane, R., Levron, Y., & Maksimovic, D. (2014). "Active balancing system for electric vehicles with incorporated low voltage bus." 2014 IEEE Applied Power Electronics Conference and Exposition - APEC 2014. doi:10.1109/apec.2014.6803768

[10] Ciprian Antaloae, James Marco, Francis Assadian, "A Novel Method for the Parameterization of a Li-Ion Cell Model for EV/HEV Control Applications" November 2012 IEEE Transactions on Vehicular Technology 61(9):3881-3892

[11] M. Brandl ; H. Gall ; M. Wenger ; V. Lorentz ; M. Giegerich ; F. Baronti ; G. Fantechi ; L. Fanucci, R. Roncella,"Batteries and battery management systems for electric vehicles," 2012 Design, Automation & Test in Europe Conference & Exhibition (DATE), Dresden, 2012, pp. 971-976, doi: 10.1109/DATE.2012.6176637.

[12] Xiaochao Xiao, Xiaojun Liu, Libiao Qiao, Shuo Li, "A Li-ion Battery Management System Based on MCU and OZ8920", 2012 International Workshop on Information and Electronics Engineering (IWIEE 2012)

[13] Kim, M.-Y., Kim, C.-H., Kim, J.-H., & Moon, G.-W. (2012). "A modularized BMS with an active cell balancing circuit for lithium-ion batteries in V2G system." 2012 IEEE Vehicle Power and Propulsion Conference. doi:10.1109/vppc.2012.6422665

[14] Yinjiao Xing 1 , Eden W. M. Ma 1, Kwok L. Tsui 1,2 and Michael Pecht 1,3, "Battery Management Systems in Electric and Hybrid Vehicles" Energies 2011, 4, 1840-1857; doi:10.3390/en4111840

[15] K. W. E. Cheng, Senior Member, IEEE, B. P. Divakar, Hongjie Wu, Kai Ding, and Ho Fai Ho " Battery-Management System (BMS) and SOC Development for Electrical Vehicles", IEEE TRANSACTIONS ON VEHICULAR TECHNOLOGY, VOL. 60, NO. 1, JANUARY 2011

[16] D. Xu, L. Wang and J. Yang, "Research on Li-ion Battery Management System," 2010 International Conference on Electrical and Control Engineering, Wuhan, 2010, pp. 4106-4109, doi: 10.1109/iCECE.2010.998.

[17] Zhang Haoming, Sun Yukun, Ding Shenping and Wang Yinghai, "Full-digital lithium battery protection and charging system based on DSP," 2008 27th Chinese Control Conference, Kunming, 2008, pp. 265-268, doi: 10.1109/CHICC.2008.4605354

[18] R. Janga and S. Malaji "Performance evaluation of active clamp forward converter with fuzzy logic controller", International Conference on Intelligent Computing and Control (I2C2), Coimbatore, pp. 1-6, April 2017.

[19] Dheeraj and V. Rajini, "Comparison of active clamping circuits for isolated forward converter", IEEE 6th International Conference on Renewable Energy Research and Applications (ICRERA), San Diego, Canada, pp. 839-841, March 2017.

[20] S. Fan, J. Duan, L. Sun and Y. Han, "The balancing system of supercapacitor based on active clamped forward converter", International Conference on Circuits, Devices and Systems (ICCDS), Chengdu, pp. 29- 33, April 2017.

[21] Sudeep E, Rachappa, B. K. Singh, V. S. Chippalkatti and K. U. Rao, "Design and implementation of current mode controlled 150W miniature forward converter for defense application", IEEE International Conference on Power Electronics, Drives and Energy Systems (PEDES), Trivandrum, pp. 1-6, June 2016.